

# Chirality-Dependent Growth Rate of Carbon Nanotubes - A Theoretical Study

Heiko Dumlich\* and Stephanie Reich

*Fachbereich Physik, Freie Universität Berlin, 14195 Berlin, Germany*

(Dated: October 30, 2018)

We consider geometric constraints for the addition of carbon atoms to the rim of a growing nanotube. The growth of a tube proceeds through the conversion of dangling bonds from armchair to zigzag and vice versa. We find that the growth rate depends on the rim structure (chirality), the energy barriers for dangling bond conversion, and the growth temperature. A calculated chirality distribution derived from this minimalistic theory shows surprisingly good agreement with experiment. Our ideas imply that the chirality distribution of carbon nanotubes can be influenced by external parameters.

PACS numbers: 61.48.De, 61.46.Fg, 81.07.De, 81.10.Aj

## I. INTRODUCTION

The properties of carbon nanotubes [1] depend strongly on their chirality or atomic structure. Most notably, the metallic and semiconducting character and the band gap of a tube change with  $(n, m)$  chiral index. One of the greatest challenges in nanotube research and application is to control the chirality during the growth. This would allow the production of tubes with tailored properties without relying on a sorting of bulk samples.

The growth of a nanotube can conceptually be divided into two stages: the nucleation of a cap and the elongation of the nucleus into a tube [2–6]. Reich *et al.* [7] showed that the nucleation of the cap fixes the chirality of an individual tube as a change in chirality is unlikely during the growth phase. Harutyunyan *et al.* [8] reported preferential growth of metallic tubes and claimed the selection to follow from the shape of the catalytic particles, i.e., chirality selection during the nucleation phase.

The final volume fraction of a given nanotube type does not only depend on the nucleation, but also on growth speed during elongation. Elongation was mainly studied in simplistic models with carbon addition [9, 10]. Ding *et al.* [11] argued that achiral armchair and zigzag tubes grow by introducing kinks when starting a new layer. They predicted the armchair kinks to require much less energy than zigzag kinks. The growth process, which is driven by a monotonous decrease in free energy during elongation, will, therefore, favour armchair tubes. Within this line of reasoning chirality selection is independent of external parameters such as catalyst type and temperature.

In this paper, we suggest that the chiral-angle distribution of carbon nanotubes depends on external parameters. The key is to manipulate the energy difference between armchair and zigzag dangling bonds through the choice of metal catalyst and growth conditions. We arrive at this conclusion by looking at the geometry of a growing tube, the number and types of places for carbon addition. The rim of a nanotube consists of three different growth sites with a varying energy barrier for the

addition of carbon atoms. The number and distribution of growth sites is a function of chirality. Combining this minimalistic geometric approach with calculated energy differences for carbon dangling bonds on metals we predict a distribution of chiral angles that is in surprisingly good agreement with experimental findings.

This paper is organized as follows. We first show how growth proceeds with carbon addition with respect to our model, Sec. II A. The essential properties of rims made up by hexagons are discussed in Sec. II B. The growth factor, which allows us to understand why chiral selectivity occurs during the nanotube elongation, is introduced in Sec. II C. We then discuss how the chirality distribution can be influenced by external parameters in Sec. II D. Finally, in Sec. III we use our model - derived in Sec. II - to obtain two exemplary chirality distributions and compare our results to experimentally determined data. Section IV summarizes this work.

## II. MODEL

### A. Growth

Let us first consider schematically the growth of a carbon nanotube. In Fig. 1 we present a 3d wire model of a possible growth route of a  $(5, 5)$  nanotube. The growth proceeds through to addition of  $C_2$ . The first carbon atom adds endothermically and is followed exothermically by a second carbon atom. The pentagon created in the first step is energetically less favorable than hexagons. We, therefore, expect the next carbon atom to be added to the pentagon. Also, the creation of more and more pentagons would close the tube and terminate growth [12]. Alternatively, a carbon dimer is added.

Going through the series of tubes in Fig. 1a) to d) a layer of carbon atoms was grown, which corresponds to half a unit cell of the  $(5, 5)$  tube. The continuation of the process - until growth is terminated - leads to an armchair carbon nanotube. In the lower panels of Fig. 1a) to d) we introduce a schematic representation of the grow-

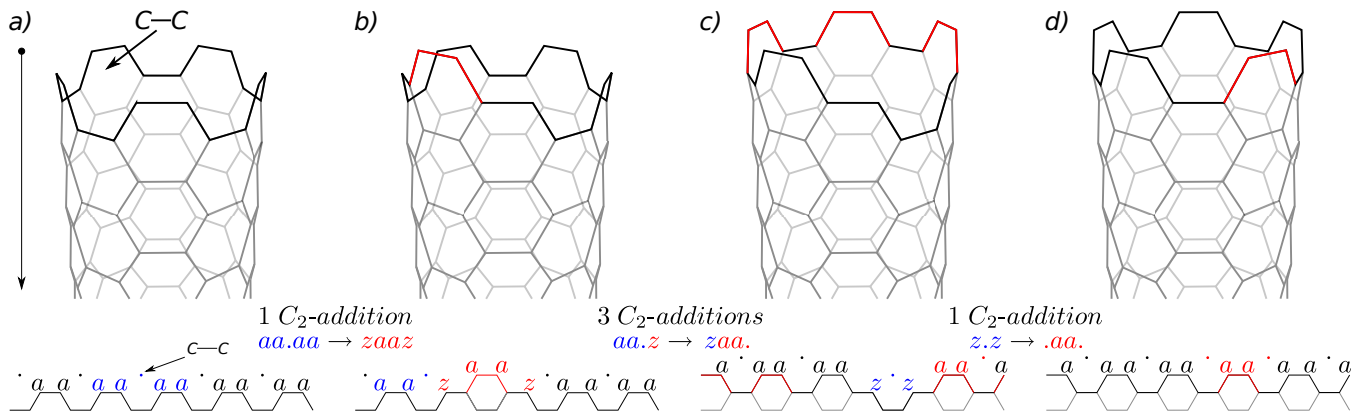


FIG. 1: Three dimensional (top) and reduced rim (bottom) representations of half layer growth of a (5,5) carbon nanotube. The reduced rim representations at the bottom are obtained by unzipping the 3d wire model (top). The “.” denotes a growth site for  $C_2$  addition, the  $a$  stands for an armchair and the  $z$  for a zigzag dangling bond. The arrow at the left denotes the growth direction. We assume root growth, but the picture is turned upside down and a catalyst was omitted for clarity of the  $C_2$  addition. *a)* A  $C_2$  adds at the rim. The induction of a new layer is accompanied by a barrier [11]. *b)* 3  $C_2$  additions follow without experiencing an energy barrier leading to tube *c)*. The last  $C_2$  addition leads to a stable rim or closed layer. *d)* A half layer is grown compared to *a)*. This process continues until the growth is terminated.

ing rim of a nanotube. The reduced rim representation unfolds the rim of the tubes in two dimensions. The “.” denote growth sites at which the addition of  $C_2$  is energetically favorable because a hexagon is created. The  $a$  stands for an armchair dangling bond; it consists of one of two neighbouring twofold C-C bonded atoms. The  $z$  stands for zigzag dangling bond; it has two saturated C neighbours and is itself twofold C-C bonded.

The first  $C_2$  addition to the rim starts a new layer by converting two  $a$  into  $z$  dangling bonds, which is accompanied by an energy barrier [11], compare Fig. 1*a)* and *b)*. The following three  $C_2$  additions do not change the energy of the rim, since they only move  $a$  and  $z$  dangling bonds leading to Fig. 1*c)*. The final  $C_2$  addition to Fig. 1*c)* yields a finished armchair layer presented in *d)*. We argue that the conversion and movement of the growth sites and the energetic barriers for the conversion determine the chirality-specific growth speed of carbon nanotubes.

## B. Rim

In the following we first discuss the essential properties of rims made up by hexagons. All carbon nanotube rims consist of armchair  $a$  and zigzag-type dangling bonds  $z$ . The number and nature of the dangling bonds in a rim depend mainly on chirality  $(n, m)$ . The rim that follows most closely the chiral circumferential vector of a tube has  $N_a = 2m$  armchair and  $N_z = n - m$  zigzag dangling bonds. For the (5,5) armchair tube this rim is shown in Fig. 1*a)*. During the growth the total number of dangling bonds in the rim remains constant  $N_a + N_z = n + m$ , while  $N_a$  and  $N_z$  vary. By this condition we include

TABLE I: Overview of the three growth site types with “Δ.” the change in the growth site number, “transition” the change of the bond structure and examples for the transitions.

growth site	Δ.	transition	example
$aa.aa$	-1	$aa.aa \rightarrow zaaaz$	Fig.1 <i>a)</i> → <i>b)</i>
$aa.z/z.aa$	0	$aa.z \rightarrow zaa./z.aa \rightarrow .aa.z$	Fig.1 <i>b)</i> → <i>c)</i>
$z.z$	+1	$z.z \rightarrow .aa.$	Fig.1 <i>c)</i> → <i>d)</i>

all reasonable configurations of a growing nanotube and exclude obviously unreasonable configurations, e.g., one side of the tube being much longer than the other side.

Following the rims in Figs. 1*a)*-*d)* from left to right leads to the notation of the particular configuration of a rim: *a)*  $.aa.aa.aa.aa.aa$ , *b)*  $.aa.zaaaz.aa.aa$ , *c)*  $a.aa.aaz.zaa.a$ , and *d)*  $a.aa.aa.aa.aa.a$ . A rim thus consists of a combination of  $z.z$ ,  $aa.z$ ,  $z.aa$  and  $aa.aa$  growth sites. The  $aa.z$  and  $z.aa$  growth sites are identical by symmetry. The  $aa$ ,  $za$ ,  $az$ , and  $zz$  configurations do not contain a growth site as  $C_2$  addition does not add hexagons. Therefore, they do not contribute to the tube elongation process. In the starting configuration the number of growth sites in a rim of an  $(n, m)$  nanotube is  $N_{aa.aa} = 2m - n$ ,  $N_{aa.z} = \min(m, n - m)$  with “min” the minimum and  $N_{z.z} = 0$ . Note that for tubes with  $2m - n \leq 0$  there are only  $aa.z$  growth sites and zigzag tubes ( $m = 0$ ) do not contain any growth sites at all. The growth of zigzag tubes is suppressed in our model and needs an intermediate addition of C or  $C_3$  to induce a growth site for  $C_2$  addition, that we do not consider here. A  $C_2$  addition to the rim will change the type and the number of growth sites, see Tab. I.

### C. Growth Factor

The rim of an  $(n, m)$  nanotube with  $n > m > n/2$  can be divided into a part with a chiral vector  $(2m - n, 2m - n)$  that contains  $aa.aa$  growth sites and a part with a vector  $(2n - 2m, n - m)$  that consists exclusively of  $aa.z$  sites. Therefore, all nanotube rims can be divided in  $aa.aa$  containing rim parts and  $aa.z$  containing rim parts. During the growth the number of growth sites contributed by a rim part containing exclusively  $aa.z$  sites remains constant. The number of growth sites contributed by a rim part containing exclusively  $aa.aa$  sites, however, changes continuously during the growth as is best illustrated by the example of an armchair tube. Growing a full layer of an armchair rim requires the addition of  $2 \cdot (2m - n) = n + m$  carbon dimers. The maximum number of  $aa.aa$  growth sites  $2m - n$  occurs only at half and full armchair layers. The other  $2 \cdot (2m - n) - 2$  growth steps have one growth site less[23]. Summing up the number of growth sites in each step and dividing by the number of  $C_2$  additions yields the average growth site number

$$\Lambda_{aa.aa}(n, m) = 2m - n - 1 + \frac{1}{2m - n}. \quad (1)$$

Similarly, we find the average growth site number for the rim part containing  $aa.z$  sites  $\Lambda_{aa.z} = N_{aa.z}$ . Adding the contributions of  $aa.aa$  and  $aa.z$  rim parts yields the average number of growth sites as a function of chiral indexes  $n$  and  $m$

$$\Lambda(n, m) = \begin{cases} \Lambda_{aa.aa} + \Lambda_{aa.z} & \text{if } 2m - n > 0 \\ \Lambda_{aa.z} & \text{otherwise.} \end{cases} \quad (2)$$

The addition of  $C_2$  dimers to the  $\Lambda(n, m)$  sites will lead to a lengthening of the tube with  $n + m$   $C_2$  additions for a single full layer. If we define the abundance of a certain nanotube chirality to depend on the number of full carbon layers, we find the growth speed of a tube to be proportional to

$$\Gamma(n, m) = \frac{\Lambda(n, m)}{n + m}. \quad (3)$$

The growth factor  $\Gamma(n, m)$  allows us to understand why chiral selectivity occurs during the nanotube elongation phase. In the following we will show how we can influence the chiral distribution during the elongation of a nanotube.

### D. Influence on Chirality Distribution

The addition of  $C_2$  to the different growth sites will experience varying energy barriers, as zigzag dangling

bonds ( $E_z = 2.90$  eV) require much more energy than armchair dangling bonds ( $E_a = 2.10$  eV) in vacuum [13]. The armchair configuration is energetically favorable because it consists of two dangling bonds on neighbouring C atoms that form a triple bond. To model experimental growth conditions we need to consider a metal catalyst in most growth scenarios. The energetic difference between  $a$  and  $z$  dangling bonds is reduced by the presence of a metal [6, 7, 11], as carbon-metal bonds are formed. However, the difference remains non-zero, as electrons of carbon neighbours influence the total bond energy of the carbon-metal bonds, rendering  $a$  lower in energy than  $z$ .

The energy barrier for the  $C_2$  addition to an  $aa.aa$  site depends on the conversion of  $aa.aa$  into  $zaaz$  dangling bonds (see Tab. I). The conversion requires an energy

$$\Delta_a = E_{zaaz} - E_{aa.aa} = 2E_z - 2E_a = 2E_a(r - 1) \quad (4)$$

with  $E_a$  the energy of an armchair and  $E_z$  the energy of a zigzag dangling bond. With  $r = E_z/E_a$  we denote the ratio between the two energies. The total dangling bond energies as well as their ratio depend on the catalyst. Changing  $z.z$  into  $.aa.$  we gain  $\Delta_a$ . In contrast growing at an  $aa.z$  site will cost no energy; this growth happens without an energetic barrier. This energetically different behaviour allows to affect the chirality distribution of carbon nanotubes through external parameters such as the metal catalyst and the growth temperature.

If the addition to  $aa.aa$  sites has a negligible barrier ( $r \approx 1$  or  $\Delta_a \ll k_B T$ ) all growth sites can contribute to the growth speed. We combine Eqs. (3) and (2) to obtain  $\Gamma$ . Figure 2a) shows the growth speed  $\Gamma$  as area size in chiral angle and diameter dependence for diameters  $d = 0.675$ - $1.055$  nm. The highest  $\Gamma$  occur for  $(n, n)$  armchair tubes. A small trend for increasing  $\Gamma$  exists for larger diameter tubes, resulting from the fractional term of Eq. (1), as the comparison of the armchair tubes shows. Changing the environment (e.g. another catalyst with another  $r$  or adjustment of temperature) so that  $\Delta_a \gg k_B T$ , the  $aa.aa$  growth sites will not contribute anymore; Eq. (3) yields  $\Gamma = \Lambda_{aa.z}/(n + m)$ , which leads to a different growth speed distribution. The highest  $\Gamma$  now occurs for  $(n, \frac{n}{2})$  chiral tubes, see Fig. 2b).

For real samples we expect a distribution of growth speed  $\Gamma$  to be between the two limiting cases. The thermal energy of nanotube growth is on the order of  $k_B T \approx 0.05$ - $0.11$  eV [14, 15].  $\Delta_a$  depends on the catalyst material, its composition and - less pronounced - on the position of the carbon with respect to the metal atom. The barriers for metal catalysts are on the order of  $\Delta_a \approx 0$ - $0.12$  eV for various metals [7, 11] and thus comparable to the thermal energy. Therefore, the addition to the  $aa.aa$  site is not suppressed. This agrees with the results of Ding *et al.* [11], that the barrier for armchair kink introduction - which corresponds to  $C_2$  addition to  $aa.aa$  - is negligible. Recently, other materials like  $SiO_2$

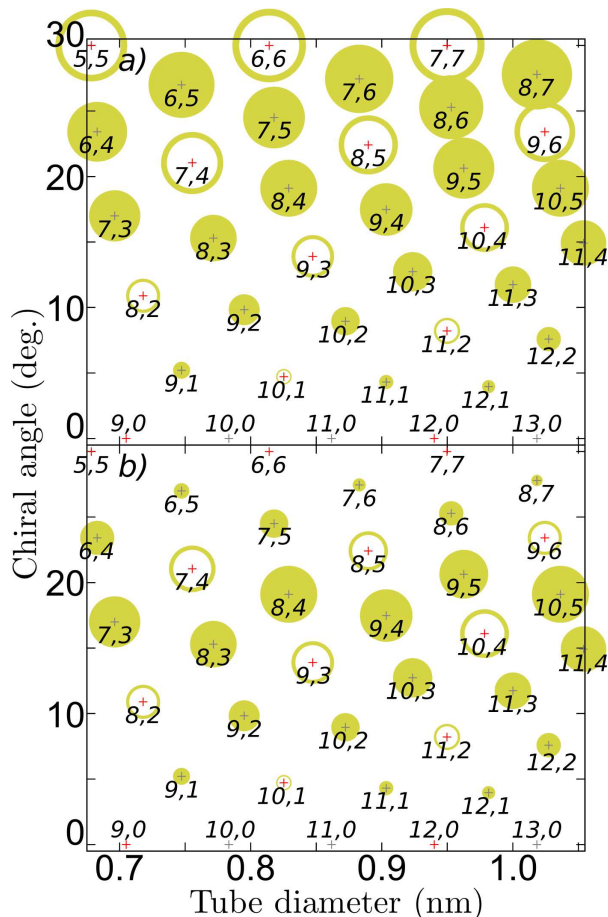


FIG. 2: Comparison of  $\Gamma(n,m)$  for tube diameters  $d = 0.675\text{-}1.055$  nm for *a)*  $\Delta_a \ll k_B T$ . *b)*  $\Delta_a \gg k_B T$ . The abundance of metallic/semi-metallic tubes (open circle, red cross) decreases compared to semiconducting tubes (full circle, gray cross) from *a)* to *b)*.

were found to catalyze nanotube growth [16]. Further, bimetallic catalysts contain different barriers and may be extremely interesting for influencing the chirality distribution [17].

### III. DISCUSSION

Up to now we concentrated on the growth of an existing nanotube nucleus. The chirality distribution of a sample will also depend on the nucleation phase, i.e., whether a particular tube cap is nucleated or not [20]. The diameter of carbon nanotubes is clearly determined by the nucleation step [21]. We now assume a distribution of chiral indices where (i) the diameter is fixed by nucleation and (ii) the chiral angle distribution is given by Eq. (3) with  $\Delta_a \ll k_B T$ . Figure 3*a)* compares the chirality distribution of semiconducting nanotubes with  $d = (0.93 \pm 0.3)$  nm to the experimental distribution in HiPco tubes; Fig. 3*b)* is for tubes with

$d = (0.75 \pm 0.15)$  nm and ACCVD samples [18]. The agreement between theory and experiment in Fig. 3*b)* is striking. Our model very well predicts the overall decrease of the number of tubes with increasing chiral angle. The strong discrepancies for selected chiralities - e.g. the strong luminescence of the (10,2) tube - is most likely due to a high quantum yield for some nanotubes [22]. On the other hand, the nucleation phase might also prefer certain chiralities [7]. It would be highly desirable to establish an unambiguous chirality distribution experimentally to clarify these points.

Figure 2*a)* verifies our assumption, that a mixture of the  $\Gamma$  factors derived for  $\Delta_a \ll k_B T$  and  $\Delta_a \gg k_B T$  have to be used for real samples as the deviation between the theoretical and experimental part of Fig. 3*a)* show. Figure 3*b)* on the other hand perfectly reproduces the trend with only considering the contribution of the  $\Gamma$  factor for  $\Delta_a \ll k_B T$ , which is expected to result from the growth conditions. We conclude that different growth conditions have indeed an influence on the chirality distributions which results during the elongation of the nanotubes.

### IV. CONCLUSIONS

In summary, we suggested how to control the nanotube growth and elongation process through the structure of the rim. Depending on the tube chirality the rim contains three different growth sites. Geometric considerations yield the growth factor  $\Gamma$ , which in turn determines the chirality distribution of carbon nanotube samples. We showed that chiral selectivity can be obtained through a combination of external parameters. Our results will be important for the understanding and tailoring of the growth process of single-walled carbon nanotubes.

### ACKNOWLEDGMENTS

We acknowledge useful discussions with J. Robertson and S. Heeg. This work was supported by ERC grant no. 210642.

\* Corresponding author: heiko.dumlich@fu-berlin.de

- [1] S. Iijima, and T. Ichihashi, *Nature* **363**, 603 (1993).
- [2] H. Amara, C. Bichara, and F. Ducastelle, *Phys. Rev. Lett.* **100**, 056105 (2008).
- [3] Y. Ohta, Y. Okamoto, A. J. Page, S. Irlle, and Keiji Morokuma, *ACS Nano* **3**, 3413 (2009).
- [4] J.-Y. Raty, F. Gygi, and G. Galli, *Phys. Rev. Lett.* **95**, 096103 (2005).
- [5] X. Fan, R. Buczko, A. A. Puretzky, D. B. Geohegan, J. Y. Howe, S. T. Pantelides, and S. J. Pennycook, *Phys. Rev. Lett.* **90**, 145501 (2003).

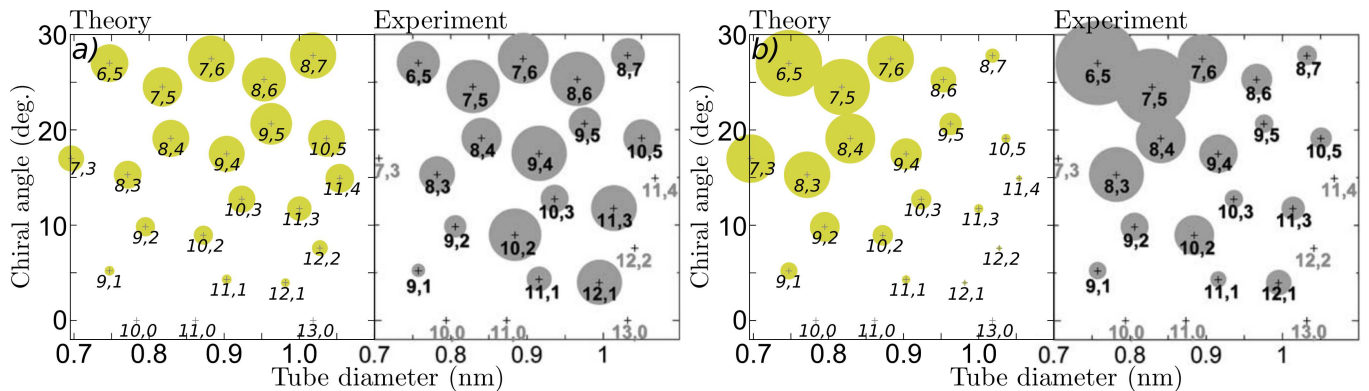


FIG. 3: Comparison of chirality distributions. Theoretically calculated distributions result from a convolution of a gaussian distribution in diameter dependence and the  $\Gamma$  factor for  $\Delta_a \ll k_B T$ . The experimentally determined chirality distributions are adapted from Miyauchi *et al.* [18]. *a*) Theory:  $d = (0.93 \pm 0.3)$  nm [19]. Experiment: HiPco sample. *b*) Theory:  $d = (0.75 \pm 0.15)$  nm. Experiment: ACCVD sample grown at  $650^\circ\text{C}$  with Fe/Co catalyst.

- [6] O. V. Yazyev and A. Pasquarello, *Phys. Rev. Lett.* **100**, 156102 (2008).
- [7] S. Reich, L. Li, and J. Robertson, *Chemical Physics Letters* **421**, 469 (2006).
- [8] A. R. Harutyunyan, G. Chen, T. M. Paronyan, E. M. Pigos, O. A. Kuznetsov, K. Hewaparakrama, S. M. Kim, D. Zakharov, E. A. Stach, and G. U. Sumanasekera, *Science* **326**, 116 (2009).
- [9] D. A. Gomez-Gualdron and P. B. Balbuena, *Nanotechnology* **19**, 485604 (2008).
- [10] Q. Wang, M.-F. Ng, S.-W. Yang, Y. Yang, and Y. Chen, *ACS Nano* **4**, 939 (2010).
- [11] F. Ding, A. R. Harutyunyan, and B. I. Yakobson, *PNAS* **106**, 2506 (2009).
- [12] Y. H. Lee, S. G. Kim, and D. Tomanek, *Phys. Rev. Lett.* **78**, 2393 (1997).
- [13] A. Thess, R. Lee, P. Nikolaev, H. Dai, P. Petit, J. Robert, C. Xu, Y. H. Lee, S. G. Kim, A. G. Rinzler, D. T. Colbert, G. E. Scuseria, D. Tomanek, J. E. Fischer, and R. E. Smalley, *Science* **273**, 483 (1996).
- [14] M. Cantoro, S. Hofmann, S. Pisana, V. Scardaci, A. Parvez, C. Ducati, A. C. Ferrari, A. M. Blackburn, K.-Y. Wang, and John Robertson, *Nano Lett.* **6**, 1107 (2006).
- [15] L. Zheng, B. C. Satishkumar, P. Gao, and Q. Zhang, *J. Phys. Chem. C* **113**, 10896 (2009).
- [16] B. Liu, W. Ren, C. Liu, C.-H. Sun, L. Gao, S. Li, C. Jiang, and H.-M. Cheng, *ACS Nano* **3**, 3421 (2009).
- [17] W.-H. Chiang and R. M. Sankaran, *Nature Materials* **8**, 882 (2009).
- [18] Y. Miyauchi, S. Chiashi, Y. Murakami, Y. Hayashida, and S. Maruyama, *Chemical Physics Letters* **387**, 198 (2004).
- [19] S. M. Bachilo, M. S. Strano, C. Kittrell, R. H. Hauge, R. E. Smalley, and R. B. Weisman, *Science* **298**, 2361 (2002).
- [20] S. Reich, L. Li, and J. Robertson, *Phys. Rev. B* **72**, 165423 (2005).
- [21] Y. Li, W. Kim, Y. Zhang, M. Rolandi, D. Wang, and H. Dai, *J. Phys. Chem.* **105**, 11424 (2001).
- [22] S. Reich, C. Thomsen, and J. Robertson, *Phys. Rev. Lett.* **95**, 077402 (2005).
- [23] The number of growth sites for other, less likely growth paths will differ somewhat from Eq. (1). However, we verified Eq. (1) to be correct within  $\pm 5\%$  (derived for the (4,4) tube in comparison to the next 4 less likely paths).